Multi Band Passive Forward Scatter Radar

S. Hristov, A. De Luca, M. Gashinova, A. Stove, M. Cherniakov
EESE, University of Birmingham
Birmingham, B15 2TT, UK
m.cherniakov@bham.ac.uk

***Abstract*— This paper describes the results of an experimental study of Forward Scatter Radar (FSR) air target detection based on the multi band signals of opportunity: FM radio, Digital Audio and Video broadcast stations. This Passive FSR (P-FSR) operation is obtained by means of a simple and robust correlation process based on self-mixing. Target detectability is discussed as a function of the carrier frequency, the target size and its height at the baseline crossing. Experimental results are shown using a wide variety of sources of opportunity, target types, baselines and receiver configurations. The target signatures obtained from the different illuminators are compared and ways of extracting the kinematic parameters of the aircraft are discussed. This validates the claimed effectiveness and robustness of the P-FSR with the presented processing scheme.**

***Index Terms* --- Aircraft detection, Forward scattering, Passive radar, Radar detection**

I. INTRODUCTION

Forward Scatter Radar is a subclass of Bistatic Radar, defined by the bistatic angle (β) close to 180º [1], [2] forming an 'electronic fence'. As known for the resolution of bistatic radar [3], both the range resolution and the Doppler (velocity) resolution becomes very poor when the forward-scatter case is approached. In this case the 'ambiguity diagram' [3] as conventionally understood becomes meaningless. The target can be almost anywhere the range-velocity space, being limited only to remain within the forward-scatter regime throughout the measurement time. It was demonstrated in [4], however, that precise estimates of the target's speed can be obtained by matched filtering the non-constant Doppler signal seen from a target as it approaches, passes through and emerges from the forward-scattering region.

The behavior of the 'known' but non-constant reference Doppler profile differs from the conventional ambiguity function which assumes a constant Doppler shift but has some analogy with the non-linear (parabolic) phase response assumed in Synthetic Aperture Radar (SAR) processing. As in the SAR case this method generates 'cross-range' (cross baseline) information, but as the target is known to be moving and the radar stationary, the FSR case yields cross-range speed rather than cross-range position. In practice in this approach to FSR target detection the Doppler processing is preceded by a conventional 'matched filter' in the fast-time domain. Such an approach uses the assumption that for the low Doppler shifts seen in this mode the signals from the broadcast transmitters can be treated as being Doppler-tolerant. This is also analogous to many forms of SAR processing. In some literature the FS coherent signal processing refers as Inverse Shadow SAR

The FS principle for target detection is the interruption of the direct signal between transmitter (Tx) and receiver (Rx) due to the crossing of their line of sight (LoS) [5]. Rather than considering FSR as a 'singular' case of a 'general' bistatic configuration, it is more useful to see FSR as a separate class of radar system. This is because the FSR target characteristics originate from different physical principles from most traditional radar. In the forward-scatter case, the target signature is obtained through the shadowing of the direct signal by the target [1], rather than reflections from it. (In practice this means that only moving targets can be detected since the receiver must look for a change in the level of the direct signal).

Using broadcasting transmitters as illuminators for passive radars meanings, which have not been designed for radar use, mean that the ambiguity function is not under the system designers control. However, this is not an issue in the forward-scatter case because of the 'explosion' of the ambiguity function in the forward-scatter case to cover all the range-velocity space. This distinctive feature defines FSR's strengths and limitations at the same time. The physical principle and topology of FSR implies that the target can only be detected when it is moving within the proximity of the baseline. Although the radar has no 'classical' resolution in this configuration, the physical principle on which these systems rely allows the detection performance to be completely independent on both the target material and shape [1]. This makes this type of radar a good counter-stealth system, which naturally makes it capable to serve as an electronic fence [6]. As well as giving a return which is independent of the target material, the target FS Cross Section (FSCS) in the optical scattering region is usually significantly bigger than its monostatic and bistatic counterparts.

As stated in [2] a FSR mode can add considerable extra benefits to the existing bistatic radar and can in practice be integrated in those systems without requiring significant changes to the hardware. One of the appealing characteristic of a P-FSR system is that, as long as the frequencies of signals of opportunity are within the receiver bandwidth, such signals may be exploited in FSR applications. When multiple baselines are available, crossing time-based techniques can be exploited for the non-ambiguous retrieval of all the kinematic parameters [7], [8]. As shown in this paper the power level is not a restriction in a wide range of situations: thus only signal frequency has a strong impact on the P-FSR performance. This significantly reduces the constraints on the range of operational waveforms which will allow such a system to function effectively.

The goal of this paper is twofold. Firstly, it presents initial results of the ongoing research. Secondly, it demonstrates the feasibility and practical applicability of P-FSR using: Digital Video Broadcasting-Terrestrial – DVB-T [9], Digital Audio Broadcasting – DAB [10], and Frequency Modulated – FM [11] waveforms of opportunity to detect airborne targets and estimate target speed. For this purpose two challenging scenarios involving small targets and non-ideal trajectories (i.e. with crossing angles significantly smaller than 90°) are considered.

The paper is organized as follows. In Section II a new simple approach to extract Doppler signature from the received signal is presented having its effectiveness analytically demonstrated for both digital (DAB and DVB-T) and analogue (FM) modulated signals. Some considerations about the received power and the influence of the target trajectory on the system performance are then discussed in Section III. Trials scenarios and experimental setups to detect various aircrafts are described in Sections IV and V together with experimental results analysis. Speed estimations for the targets, obtained from the data, are presented in Section VI. At the end of the paper, general conclusions are formulated.

II. FORWARD-SCATTER TARGET DOPPLER SIGNATURE EXTRACTION PROCESSING CHAIN

Optimal radar detection is based on correlation of the received signal with a sample of the transmitted reference signal. This same approach is used in systems using illuminators of opportunity and in FSR and also in the algorithm described here. Systems using illuminators of opportunity

(IoOs) usually have to acquire the reference signal using an antenna steered towards the transmitter. In the FSR case the reference signal (direct signal) is received in the same channel, as the surveillance signal. The algorithm described in this paper actually exploits this feature of the forward scatter geometry to operate a self-mixing between these signals.

This research has used the algorithm introduced in [12]. The approach is based on the physical operational principle of FSR, which is the amplitude modulation of the direct path (leakage) signal due to target shadowing. Hence, if we manage to extract the amplitude modulation from the detected signal, we will separate the reference signal from the target contribution.

It must be pointed out that the processing scheme considered here needs a Direct Signal to Noise Ratio (DSNR) at the input to the correlator which is significantly above 0 dB to operate properly [13], [14]. This condition is nearly always satisfied as the broadcasting transmitters can be assumed to guarantee DSNR≥10 dB anywhere within their coverage area.

The block diagram of the processing chain used to extract the Doppler signature is shown in Fig. 1. In order to extract the target information, the received signal (Point A) is multiplied with the hard-limited reference signal (Point B). It is well known [4] that for a fast oscillating function the hard-limited version is highly correlated with the original (non-limited) signal and therefore only minimal loss in the signal processing efficiency is expected from using this scheme.

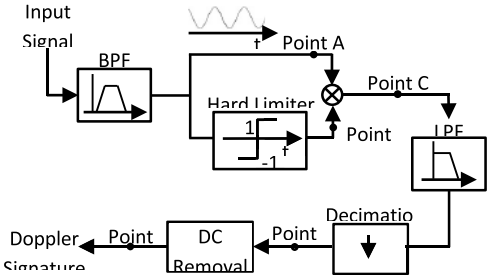

Figure 1 –Algorithm block diagram.

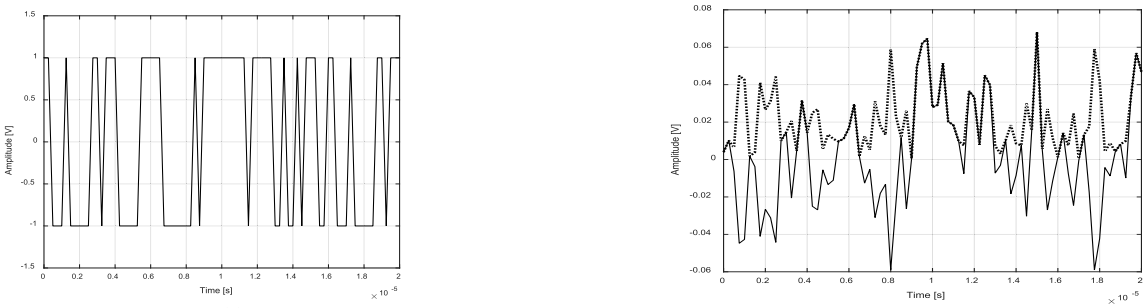

(a) (b)

Figure 2 –Hard limiter response (a). Signal at point A (b) – solid line) and signal at point C (b) – dashed line.

Such multiplication when applied to real signals is mathematically equivalent to the extraction of the absolute value of the signal at Point A [15].

The output signal is then low pass filtered by LPF which is designed to leave only frequency components which are within the range of the expected Doppler frequencies from targets which are close to the baseline, as discussed below. The amplitude modulation rate due to passage of the target through the baseline is lower than the range of these Doppler shifts.

If the Doppler shifts are considered only within the Main Lobe (ML) of the FSCS then the target speed can be assumed to be constant within such a narrow scattering period and for a linear trajectory, its upper limit [2] is expressed by (1):

$$f_{D,FS} \leq \frac{v_{tg}\cos(\delta)}{2D} \qquad (1)$$

where v_{tg} is the speed and δ is the inclination of target trajectory with respect to the bistatic angle bisector. D is the effective target shadow aperture dimension. In order to estimate the upper limit of the expected Doppler frequency for an airborne target, the value of D in (1) should be taken as the smallest value of either wing span or body length [2].

If, however, the target FSCS sidelobes are included into the overall forward scatter Doppler signature they can potentially deliver richer information to be used for target classification [16]. As with any other type of Doppler radar, the filter design thus depends on the scenario and on the range of targets which must be detected.

Thus for our purpose higher Doppler shifts than the bare minimum are considered. For instance in the case of DVB-T signal of opportunity, for a 35 m airliner with a typical cruise speed of 600 km/h the maximum Doppler frequency $f_{D,FS}$ within the main lobe corresponds to orthogonal crossing and is around 2 Hz according to (1). On the other hand, recalling the bistatic Doppler frequency formula $f_D=(2v_{tg}/\lambda)\cos(\delta)\cos(\beta/2)$ [17], where λ is the wavelength of the transmitted signal and considering bistatic angles close to the forward geometry (for instance taking $\beta=175°$), the Doppler frequencies would be up to 30 Hz. Thus considering the Doppler bandwidth to be of order of tens of Hertz the LPF cut off frequency is set to 100 Hz for all the considered signals to just exceed minimum required Nyquist criterion. This means that for instance if the DVB-T B=10MHz channel is considered, after the LPF the bandwidth will become B_2=100Hz, and a 50 dB SNR gain will be expected (i.e. a noise bandwidth reduction of $B/B_2=10^5$ meaning 50 dB less noise power).

The signal obtained at the output of the LPF is the target Doppler signature. The last two blocks of the processing chain consist of the decimation, which reduces signal sample rate in proportion to its effective bandwidth, and the cancellation of the DC component. A further processing stage (not explicitly considered here) is the matched filter compression which may provide us a further integration gain of $\frac{B_2}{1/T_{\text{int}}} = 1000 \Rightarrow 30$ dB, due to the further bandwidth reduction proportional to the visibility time. Such a visibility time, due to coherency and non-fluctuating targets, in FSR is coincident with the integration time T_{int} (typically around 10 s) since the filter operation is a form of coherent integration.

The final matched filtering with the overall Doppler signature of the target will substantially recover any 'loss' due to making the low-pass filter in Fig. 1 wider than necessary, so the design of the latter is not critical to the performance of the system.

III. POWER BUDGET ESTIMMATION

As stated above the main goal of this work is to investigate the performance of passive FSR for the detection and the estimation of the kinematic parameters of airborne targets. Therefore, in this subsection we give our attention to a preliminary estimation of the power budget needed to guarantee the system efficiency.

A. FSCS Patterns

1. *Analytical Characterisation*

An important parameter which characterizes the extent of the forward scatter main lobe (ML) is its -3dB beamwidth, which is given by [2]:

$$\theta_{FSML} = \lambda / D \qquad (2)$$

Therefore, depending on the target's electrical dimensions, its flight height and the ranges to the transmitter and the receiver, there might be situations when the receiver is not illuminated by the main FS lobe. The widths of the FS main lobe for a Cessna 172 estimated by both analytical formula (2) and full-wave modelling at frequencies of broadcasting IoOs are given in Table 1 in Section A.3. More information for a range of targets and frequencies can be found in the reference [2].

Fig. 3 shows the general FSR situation when an airborne target moves through the area between Tx, at height h_t, and Rx, at height h_r, separated by the baseline L in a flat earth model approximation. This baseline is obtained as the projection of the LoS between Tx and Rx onto the earth's surface.

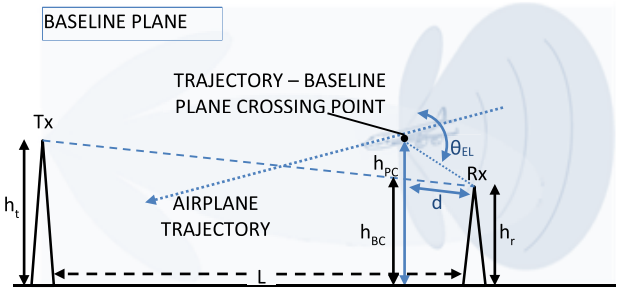

Figure 3 – FSR aircraft crossing geometry: target minimum distance from the receiver at the crossing.

The width of the forward scatter main lobe (FSML) in elevation, θ_{EL}, is given by using (2) with the target vertical dimension being used as the value for D. Since the receiver is within the FSML, even though the target does not strictly cross the baseline, its forward-scatter signature can still be detected.

It is worth noting that the receiver may also capture signals re-irradiated within the target side lobes with reduced scattered power. With this in mind, the minimum distance the target has to be from the receiver to be detected can be approximated for low target altitude as (2).

$$d = \frac{h_{PC} - h_{BC}}{\tan(\theta_{EL}/2)} = \frac{\Delta h_C}{\tan(\theta_{EL}/2)} \qquad (3)$$

In (3) the baseline inclination has been assumed negligible since in most cases the angle is of the order of fraction of degree.

The peak value of the FSCS is [1]:

$$\sigma_{FS\max} = 4\pi \frac{A^2}{\lambda^2} \qquad (4)$$

The comparison between equations (2) and (4) suggests that the choice of the operational frequency is a compromise between having a wide main lobe and maximizing the peak gain in the forward scatter direction. In particular, the use of higher frequencies to guarantee a higher power level at the receiver would result in a more stringent constraint on the maximum altitude at which the target can be detected. Multi-frequency operation can thus deliver enhanced performance in terms of both coverage and SNR. This can be easily achieved by means of passive systems exploiting broadcasting without any effort to build a transmitter able to synthesize such range of frequencies at the same time.

2. *Electromagnetic Modelling*

Simulation of RCS of a small aircraft, a Cessna 172, has been carried out using CST Microwave Studio [18]. This type of aircraft was modelled since it was used as a test target in some of the experiments (described in section V.A below). Fig. 4 (a) shows the CAD model of the target and Fig. 4 (b) shows the CST model of its RCS at 223 MHz, i.e. a DAB frequency.

The figure also indicates the horizontal plane wave illumination broad side onto the target plane cut. This corresponds to the baseline plane in Fig. 4 where θ is the elevation angle (defined as negative below horizontal). In order to simulate RCS of aircraft at particular altitude with respect to the transmitter the angle of illumination was varied from -2° to 5° with 1° intervals. This range of angles matches the geometry of the experimental scenarios.

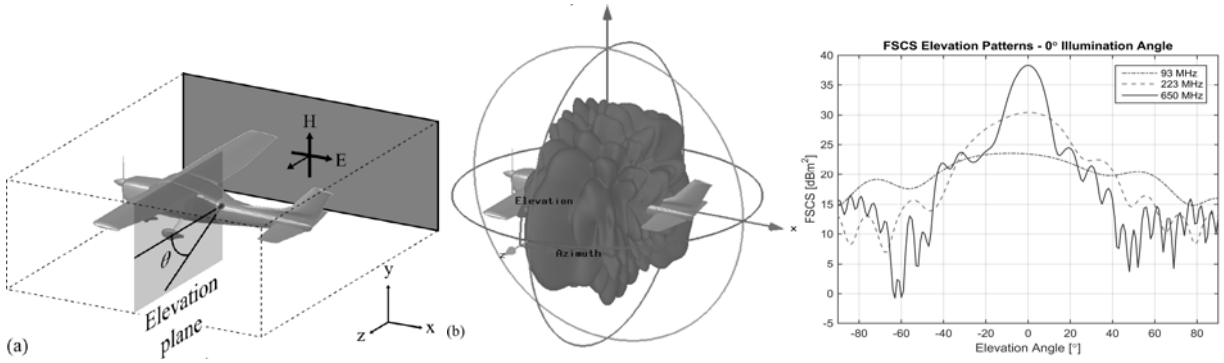

Figure 4 – (a) CST model of Cessna 172 (b) 3D RCS simulated at 223 MHz shown for 0° illumination angle (c) FSCS elevation patterns for three frequencies with a target illumination angle of 0° elevation is the FS direction.

The simulations have been made at frequencies of 93 MHz, 223 MHz and 650 MHz corresponding to FM radio, DAB radio and DVB-T signals.

An example of the 3D RCS for 0° angle of illumination is shown in Fig. 4 (b). For this study, the elevation plane of the RCS pattern, as defined in Fig. 4 (a), is of importance. Fig. 4 (c) shows 2D RCS pattern at this plane for a target illuminated at broad side (0° angle of illumination), for each frequency of interest. It should be noted, however, that the forward-scatter regime can be considered to extend to about 40° either side of broadside, even at higher frequencies. At those angles the FSCS is actually similar at all wavelengths, being the edge of lower (but wider) pattern at low frequencies and the sidelobes of such higher (but narrower) pattern seen at higher frequencies, at the same power level.

3. Comparison of Analytical Approximation and Modelling

Table 1 confirms the substantial agreement between the theoretical values obtained by (2) and (4) and the simulations of the FSCS pattern obtained from the accurate CST model.

Table 1 – Simulated (CST) and analytical (an.) FSCS results

Parameter of FSCS	**93 MHz**		**223 MHz**		**650 MHz**	
	CST	An.	CST	An.	CST	An.
θ_{EL} [deg]	70.4	79.7	36.9	33.6	13.5	11.5
$\sigma_{FS\,max}$ [dBm^2]	23.5	23.25	30.43	30.76	38.35	40.1

Given the FSCS values and elevation patterns for different illumination angles, it is now possible to make some estimation of sensitivity and of the maximum altitude at which target can be detected as shown in Section III.B.3.

B. Preliminary Power Budget

In a typical scenario where the transmitted wave is propagating above the surface there are two signals at the receiving point: direct path or LoS signal and the signal reflected from the ground. The Two Ray Path model [19] is therefore used as a reference model for the estimation of the power level received at a distance d from the transmitter (5):

$$P_{DS} = 4P_t G_t G_r \left(\frac{\lambda}{4\pi d}\right)^2 \sin^2\left(\frac{2\pi h_t h_r}{\lambda d}\right) \quad (5)$$

where P_t is the transmitted power, G_t and G_r are the transmitter and receiver antenna gains and h_t and h_r are the heights of the transmitting and receiving antennas above the local ground surface. The surface is assumed to be flat and smooth.

The target scattered signal power level can be calculated with the same model applied to the target signal as discussed in [19]:

$$P_{tgt} = 16P_t G_t G_r \sigma_{fs} \frac{1}{d_t^2 d_r^2} \frac{\lambda^2}{(4\pi)^3} \sin^2\left(\frac{2\pi h_t z_{tgt}}{\lambda d_t}\right) \sin^2\left(\frac{2\pi h_r z_{tgt}}{\lambda d_r}\right) \quad (6)$$

where z_{tgt} is the altitude of a point like target, d_t and d_r are the distances to the target from the transmitter and the receiver respectively and σ_{fs} is the target FSCS.

The power budget analysis considers a system with the parameters shown in Table 2.

Table 2 – Parameters used in the power budget evaluation.

PARAMETER	VALUE
f_c (DVB-T)	650 MHz
Δf	8MHz
P_t	50 dBW
G_t	0 dBi
G_r	8 dBi
h_t	270 m
h_r	1.5 m
z_{tgt}	200 m
σ_{fs}	10 dBm^2
T_{int}	10s
L_e	10dB

1. Direct Signal Reception Range

It is appropriate first to calculate the signal to noise ratio for the direct path signal. This is given by

$$DSNR = P_{DS} - N - L_e \quad (7)$$

where N is the receiver noise power in the signal bandwidth, L_e represents the miscellaneous losses and all the values are in dBm or decibels.

This equation allows us to evaluate the maximum possible separation between transmitter and receiver. If the direct signal (which is usually stronger than signal scattered from the target) cannot be received, then we will not be able to detect the scattered signal. The noise power is given by $N'=kTN_f\Delta f$ where k=1.38 10^{-23}J/K is the Boltzmann constant, T=290K is the system temperature, N'_f=6dB is the receiver noise figure and Δf is the frequency interval of interest, which in our case is the 8 MHz DVB-T signal bandwidth. The results of the *DSNR* calculation are presented in Fig. 5. The *DSNR* is shown by the solid curve. The dashed line represents the minimum signal to noise ratio, the threshold value which has been set to 10 dB for efficient processing (see section II.A and [13]). The intersection between these lines indicates that the maximum distance at which the DVB-T coverage is guaranteed is 300 km. It should be remembered, however, that a 'flat earth' model is used and in practice the earth's curvature will limit the maximum baseline length to around the horizon. For radio frequency signals the horizon will be at around 70 km since the effective radius of the earth at these frequencies can be taken as 4/3 of its geometrical value.

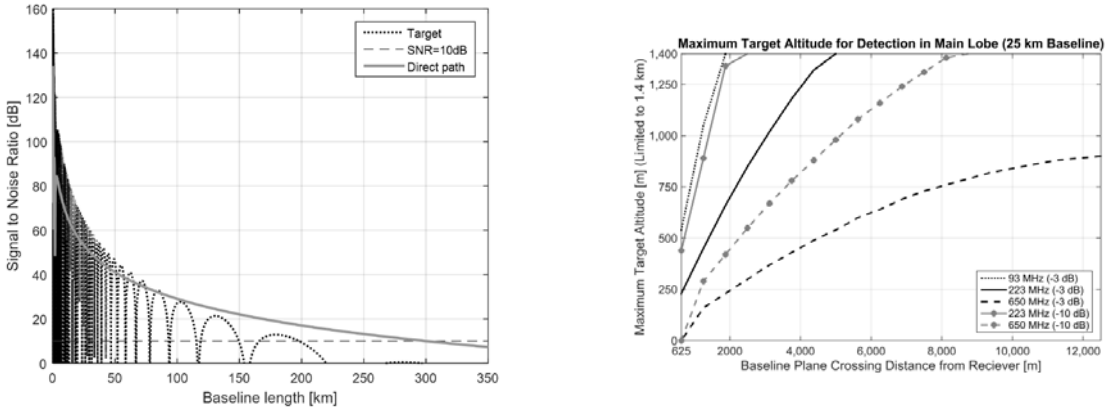

(a) (b)

Figure 5 – (a) Signal to Noise Ratio for the direct signal (dot dashed curve) and for the Target signal (solid curve). The dashed curve highlights the lowest received power level to have DVB-T coverage and to guarantee good detection performance. (b) Maximum target altitude for detection within -3dB (lines without markers) and -10 dB (lines with markers) FSCS main lobe as a function of the distance from the receiver and frequency of illumination.

2. Target Detection Range

The power of the signal scattered from the target will be considered for the worst case scenario: i.e. a very small target (see Fig. 4(c) – σ_{fs}=10dBm^2) which crosses the baseline at the midpoint, i.e. $d_t = d_r = d_m = L/2$, because it results in the minimum of the scattered power as $P_{tgt} \propto 1/(d_r^2 d_t^2)$. In this case $SNR = P_{tgt} - N_0 - L$ where N'_0 is the noise power after matched filtering (which by definition gives the best potential SNR), so the bandwidth is the inverse of the visibility time (T_{int}) (i.e. Δf=0.1Hz) and all the values are in dBm or decibels. The result using values in Table 2 is shown in the solid curve in Fig. 5. It is apparent that an *SNR* of 10 dB is attainable for baselines up to 150-200 km in this flat earth scenario. Considering fading margin of 10 dB, this will be reduced to 100-150 km still suitable for the wide area surveillance.

3. Maximum Target Altitude

We may assume that detection occurs if the FS main lobe is directed towards the receiver down to -3 dB or -10 dB off axis levels. A single baseline length of 25 km is considered here. The maximum target altitude z_{tgt} is estimated for different target crossing distances d_R from the receiver starting from the middle (see Fig. 3). The transmitter height of 270.5 m corresponds to that of the broadcast transmitter in Sutton Coldfield, UK (Section IV) and the maximum altitudes are capped to 1.4 km to limit the range of simulation required. For the lowest frequency (FM radio), the -10 dB result is not shown as the target main lobe is always visible to the receiver for the altitudes considered here. This is also true for the -3dB ML, except for when is very close to the receiver, and the same is true for the DAB frequency when considering the -10 dB lobe width. However, at this frequency, detection within the -3 dB width at the maximum altitude of 1400 m is only attainable at crossing distances of more than 5000 m from the receiver.

The effect of the narrowing of the main FSCS lobe at DVB-T frequencies (650 MHz) for this baseline length dramatically reduces the maximum target detection altitude: specifically, when considering the -3 dB width, the maximum altitude reaches about 900 m for the mid-point baseline crossing.

The above analysis assumes that detection is always possible given the FSCS values obtained. For increased baseline lengths, which may involve detection at longer ranges, higher frequency passive signals would be preferable. In fact, due to the increase in FSCS, the limitation of narrower main lobe width is compensated by the reduction in angles due to the longer baseline length itself.

The analysis has not considered how the elevation coverage of the transmitter affects the coverage. [20] suggests that the designed elevation coverage of DVB-T transmitters may limit the effectiveness of such signals for detection of targets at higher altitudes, but [21] shows experimental results that are better than [20] would suggest, a phenomenon which is perhaps attributable to the actual installed elevation patterns of the transmitters being rather less well controlled than would be expected from the laboratory.

IV. MEASUREMENTS. AIRLINER TRIALS

A. Radar system set up

A single baseline passive FSR system was set up to test the performance of the algorithm described in Section II. The Sutton Coldfield, UK broadcast transmitters [22] were used as illuminators of opportunity. Its antennas are 440m above sea level (a.s.l.), which corresponds to a 270m tower and 170m terrain height. The station broadcasts analogue and digital signals for both radio and television services with the parameters shown in Table 3. This transmitter was chosen because of its wide range of transmitter frequencies and their high power levels.

The experimental receiver of the University of Birmingham (UoB) was designed around a National Instruments USRP-2950R [23] software defined radio which contained two full-duplex transceivers, controlled by a host laptop running LabView.

Table 3 – Sutton Coldfield transmitted signals used in our experiments with their frequencies and powers.

Signal	Frequencies [MHz]	Signal Bandwidth [MHz]	Transmitted Power [kW]
FM	88.3 90.5 92.7 95.6 96.4 97.9	0.150	250 250 250 11 10 250
DAB	222.06 225.65	1.536	8.7 10
DVB-T	650 674	8	200 200

Parameters of the receiver are summarized in Table 4. During the initial experiments only DVB-T and FM signals were exploited, while for those described in Section V.B DAB signals were also used.

In each recording a pair of signals (i.e. either DVB-T & FM, or DVB-T & DVB-T) was acquired simultaneously by the two USRP receiving channels. One of the constraints imposed by the USRP is that both acquired channels must be sampled at the same rate. This is obviously set by the signal with the larger bandwidth. In our case this corresponds to the 8 MHz bandwidth of DVB-T. In order to make acquisitions in the most efficient way we decided to record signals in both USRP channels with over 10 MHz bandwidth, which is slightly larger than the DVB-T channel width. So the final sampling rate was 20 MHz for each RF channel. For both USRP channels, the center frequency was chosen to allow recording of as many available broadcast channels as possible. Thus all six FM frequencies, shown in Table 3 were recorded simultaneously.

In the two scenarios of the experiments presented in this paper, the receivers were placed so as to provide far field operation at all the frequencies used. Moreover, we are interested in operating in the optical scattering regime to exploit the increased FSCS (4) in order to deliver the required detectable power of the scattered signal. The above conditions are satisfied if:

- the target size is significantly smaller than its distances from both the Tx and the Rx. This means that both distances must be greater than the Fresnel length $S=D^2/(4\lambda)$ [15] and
- the target dimensions are much bigger than the signal wavelength, i.e. the target is electrical large: $D/\lambda>>1$ [2].

Table 4 – Parameters of the UoB experimental receiver

Tunable frequency range	50 MHz-2.2 GHz.
Antennas	DVB-T – Yagi, gain – 8 dBi; DAB – three element DAB commercial antenna gain – 6.2 dBi FM – Yagi FM antenna Gain – 5dBi
Number of channels	2
USRP channel bandwidth	10 MHz
Azimuth coverage	DVB-T- 20˚; DAB – 60˚; FM - 110˚
Elevation coverage	DVB-T- 20˚; DAB – 60˚; FM - 70˚

Table 5 –Fresnel parameter Estimation.

Signal	**Fresnel parameter *S* [m]**	**Target Electrical Dimension**	**Forward scatter main lobe FS ML [Deg]**
FM [90 MHz]	86.7	10.2	$(\theta_h , \theta_v)= (5.6;16.3)$
DVB-T [650 MHz]	626.2	73.7	$(\theta_h , \theta_v)=(0.8;2.3)$

IV.B. The largest *S* is defined by DVB-T signal frequencies and requires that the receiver to be at a minimum distance of 626.2 m from the crossing point.

On the other hand, the optical scattering condition will be less easily satisfied at FM signal frequencies for smaller aircrafts, discussed in the Section V.A, B, as is also apparent from the FSCS peak gain shown in Fig. 4 (c). This case is closer to Mie scattering, but does not significantly affect the results of detection.

Therefore, whereas for DVB-T we have guaranteed the strong FS CS increase within its main lobe [2] for FM we have a border line situation.

The initial experiments, presented in Section IV.B, were conducted near Birmingham International Airport (BHX), UK where we aimed to record signatures of planes taking off and landing. The crossing point was therefore at 6 km from site Rx1 and 15km from site Rx2, as shown in Fig. 6 (a). The distance between BHX and the Sutton Coldfield transmitter is about 20 km, making the baselines 26 km and 35 km to Rx1 and Rx2, respectively. In both experiments the constraint for far field operation was satisfied for all the frequencies used.

To obtain ground truth, all recorded passenger airplanes have been tracked using Flightradar24 [24], which provides information on their altitude (a.s.l.), location and speed with good accuracy. Due to the geometry between the transmitter and the airport flight path (cyan line in Fig. 6 (a)) the trajectories of each aircraft were similar, with a small crossing angle of about 15 degrees.

(a) (b)

Figure 6 – Trials topology shown in Google Earth [25] (a), receiver Rx1 site at 6km (b) distance from crossing point, with FM and DVB-T antennas.

B. Experimental results

The recorded signals have been processed using the approach described in Section II. For the DVB-T signals the pass-band of the BPF was set at the signal bandwidth (8MHz), while a cut-off of LPF was 100 Hz. For the FM signals an additional pre-processing step was undertaken which comprised separation of the different FM channels and decimation to a lower sampling rate in accordance with the Nyquist criterion for FM broadcasting channel bandwidth of 150 kHz. Then the upper cut off frequency of the BPF (Fig.1) was set to 150 kHz and for the LPF (after the hard limiter) it was set to 100Hz. The decimation block decimated signals to a fixed sampling rate of 200 Hz.

The experimental results presented in this section are Doppler signatures and their spectrograms, obtained at the output of the processing chain shown in Fig. 1 (point E), which allows visualization of the amplitude modulation due to the target crossing the baseline. The time domain signatures are shown together with the Short Time Fourier Transform (STFT) of the signatures. To ease the comparison of the spectrograms, they have been normalized so that the maximum levels of the FM and DVB-T signals are the same color.

The first experiment, with the receiver at position Rx1, providing 26 km baseline (Fig. 6 (a)), was carried out to record FM and DVB-T signals as explained in Section IV.A. Fig. 9 (a) shows the Doppler signature of an ascending plane after take-off from BHX. The aircraft was an Airbus A320 with dimensions of 33.8 m length, 11.7 m height and 34.1 m wingspan. It was at 180 m altitude when crossing the baseline. The speeds given by Flightradar24 for this takeoff phase are between 240 and 285 km/h.

Doppler signatures were extracted from all six FM channels from 88.3 MHz to 97.9 MHz and all of them are slightly scaled version of each other. To avoid dense plotting of very similar signals only two of them are shown in Fig. 9 (a). The gradual increase of the oscillation rate of the signatures due to acceleration during take-off stage is clearly visible. It is worth nothing that the signature in the 95.6 MHz channel is as clear as

the one from the 97.9 MHz channel, although the former has 14 dB less transmitter power (see Table 3). This demonstrates good robustness to a variety of situations involving different SNR's.

For comparison the signatures extracted from FM (97.9MHz) and DVB-T (650 MHz) signals are shown in Fig. 9 (b). Although there is a clear correspondence between the trends of the Doppler frequency in the two signals, with the crossing point being visible at 20 s, the Doppler frequencies of the FM signals are a factor of 6,5 lower than those of the DVB-T signals, exactly as would be expected from the ratio between their carrier frequencies. Indeed, corresponding spectrograms shown in Fig. 9 (c) and (d) shows that the maximum Doppler frequency of the signature with the FM signal is about 6 times smaller than that of DVB-T signal.

The smaller Doppler at the start of the record indicates the fact that the target speed is low at the start of the plane's ascent. Also in Fig. 9 (c) and (d), the highest signal intensity corresponds to the target FSCS ML (15s-23s for FM and 17s-22s for DVB-T) and decreases in the side lobes.

It can be seen from the color scales of the two spectrograms that the maximum of the DVB-T signals is 10 dB higher than that for the FM spectrogram. Since the effective radiated power and receiver aperture are greater for the FM signal and the receiver gains are the same at both frequencies, this difference shows that the directionality seen from the target is much bigger at the higher frequency, as predicted by (4).

The second experiment was made with the receiver positioned at Rx2, resulting in a baseline of 35 km as shown in Fig. 6 (a). On this occasion the aircraft were crossing the baseline during descent for the landing, because the wind was blowing from a different direction. Two different combinations of broadcasting signals were recorded: two DVB-T channels (Fig. 7 (e)) and one DVB-T with one FM channel.

The increased distance from the target path to the receiver slows everything down. For a given carrier frequency the Doppler will vary more slowly within the observed narrow FS area, but, since the crossing angle is the same, the angular interval for which the target is observed (and therefore the observation time) will increase. The lower rate of change of the Doppler frequency is clearly visible for the DVB-T signal and, obviously it affects the appearance of Doppler signature of FM signal, so that a very long record length is needed to reach a Doppler frequency above 1 Hz. Below this Doppler shift the spectrum is more likely to be contaminated by clutter [26].

Two simultaneously recorded signatures at two DVB-T channels centered at 650 MHz and 674 MHz respectively are shown in Fig. 10 for a Bombardier Dash8 Q-400 aircraft, with dimensions of 32.8 m length, 8.3 m height and 28.4 m wing span. According to Flightradar24 at the crossing instant it was at 236 m altitude with a speed of 263 km/h. The two signatures are very similar except for a phase difference due to the use of two physically separate antennas. The spectrogram in Fig. 7 (b) clearly demonstrates the deceleration of the descending aircraft. From the comparison of Fig. 7 (a), (b) and Fig. 7 (e) it is also seen that the combination of a crossing point closer to the middle point and the decreased FSCS value in the direction of Rx, due to the higher flight height, lead to reduction of received scattered power.

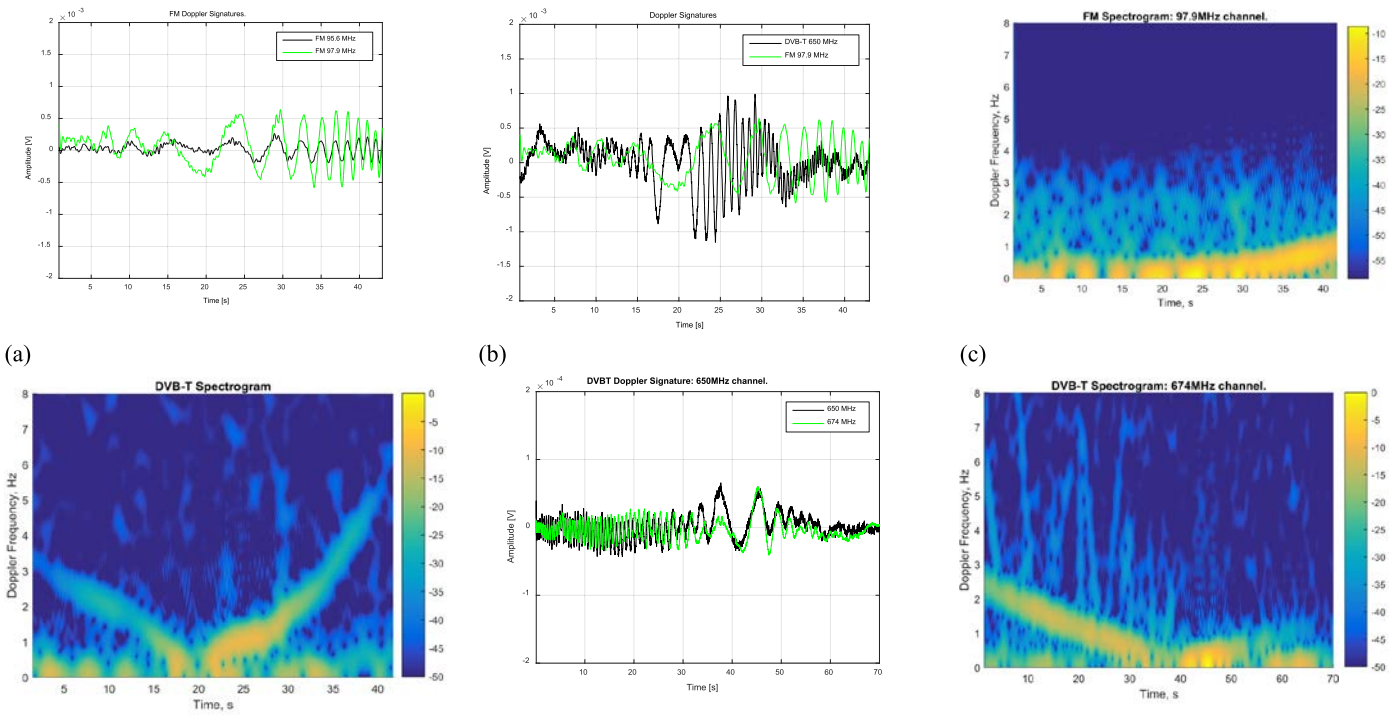

(a) (b) (c)

(d) (e) (f)

Figure 7 –FM and DVB-T Doppler signatures (a) and (b) and spectrograms (c) and (d) of the taking off Airbus A320. The baseline is 25km. DVB-T Doppler signatures (e) and spectrogram (f) of a landing Bombardier Dash8 Q-400. The baseline is 35km

V. LIGHT AND ULTRALIGHT AIRCRAFTS TRIALS

A. UoB Scenario and Results

In order to investigate the system performance for the detection of small, light, low flying aircraft, another set of experiments has been conducted for which a Cessna 172 light aircraft shown in Fig. 8 (b) was used, as a controlled target. Its dimensions are 7.3 m length, 2.3 m height and 11 m wingspan.

Table 6 – Fresnel parameter, electrical target dimensions and FS ML of the Cessna target at FM, DAB and DVB-T frequencies.

Signal	Fresnel parameter *S* [m]	Target Electrical Dimension	Forward scatter main lobe FS ML [deg]
FM [90 MHz]	9.1	3.3	$(\theta_h , \theta_v)=(17.4,83.0)$
DAB [225 MHz]	22.7	8.3	$(\theta_h , \theta_v)=(6.9,33.2)$
DVB-T [650 MHz]	65.5	23.8	$(\theta_h , \theta_v)=(2.4,11.5)$

In this experiment, the receiver was set in the open field near Sibson, close to Leicester, UK. The site is at 81.5 m height a.s.l., at 25 km distance from the Sutton Coldfield transmitter. There was a clear LoS between Tx and Rx. In addition to the receivers used for the airliner measurements, in this case, a three element DAB commercial antenna was available with a -3dB beamwidth of 60° in both horizontal and vertical planes and having 6.2 dBi gain. The site and scenario were chosen to satisfy two requirements:

1) the target can fly at a relatively low height (for rural area a limit of 450 m);
2) to be able to avoid the air traffic control constraints in the region of BHX.

The trials were conducted with the target following the 'racetrack' shown in Fig. 8 (a) which was selected, in consultation with the pilot, to cross the baseline almost perpendicularly at a point approximately one third of the way along the baseline, whilst maintaining a safe flight path.

The aircraft altitude increased by nominally 100 m on each circuit, in order to determine the system's ability to detect targets flying at different altitudes.

The results presented and discussed in this section correspond to three representative altitudes: the lowest of 450m a.s.l, the highest of nearly 1 km and an intermediate value of about 800 m as shown in Table 7. The start times of the recordings were synchronized with a GPS tracking device onboard the aircraft. The GPS ground truth data are shown in Table 7.

(a) (b) (c) (d)

Figure 8 – Trials topology on Google Earth (a); Cessna 172 ultralight aircraft (b); receiver DVB-T and DAB antennas (c); USRP and the laptop (d).

The bandwidth of the receiver used for DAB signals comprises two DAB channels centered at 222.0 MHz and 225.65 MHz (see Table 7), so, as with the FM signal, an initial processing step was incorporated to separate them. Then, after the BPF with a cut-off frequency of 750 kHz, decimation was applied to reduce the sampling rate and the LPF cut-off frequency was again set to 100 Hz.

Table 7 – GPS ground truth of three acquisitions with Cessna.

Data	Crossing distance from Rx[km]	Crossing Angle [deg]	Crossing Height a.s.l. and above baseline)[m]	Recorded Signals
D1	9.1	86	483 (354)	DVB-T + DAB
D2	9.0	87	788 (659)	DVB-T + FM
D3	7.9	85	947 (833)	DVB-T + FM

The results of the first acquisition D1 (see Table 7) at 650 MHz shows that, even though the target is much smaller than the airliner seen in the previous section, the Doppler signature in Fig. 9 (a) is well defined although the power of the scattered signal is smaller compared with that of the airliner shown in Fig. 7 (a). Moreover, the different flight stages when the target is approaching, crossing and departing from the baseline can be easily distinguished not only in the DVB-T signals but also in the DAB signatures signals in Fig. 9 (b) despite the fact that the transmitted power is 14 dB lower.

The two branches of the spectrogram in Fig. 9 (c) are symmetrical, due to the orthogonal crossing and constant speed. Moreover, the wider FS ML of the smaller target leads to an increase of the time interval in which the Doppler chirp with a frequency sweep up to 15 Hz is clearly visible.

The effect of the vertical distance, Δh_c, between the flight trajectory and the baseline (Table 7) is seen from comparison of the spectrograms of the D1, D2 and D3 data. The latter correspond to the FSML no longer impinging on the receiver, resulting in a reduced received power. The wider target FS ML seen at FM frequencies guarantees that the receiver is illuminated by the FSCS ML in a wider range of plane altitude with respect to DVB-T. However, as apparent from Fig. 4 (c), the target FSCS at 650 MHz has higher gain than for FM, not only in the main lobe but also in the first two sidelobes. Hence in the D2 and D3 acquisitions, where the target is in a lower gain region at the DVB-T frequency, but still inside the -10dB main lobe (see Fig. 6), the intensity of the FM and DVB-T spectrograms (Fig. 10 (c) and (d) – D2, and Fig. 10 (g) and (h) – D3) are comparable, as expected from Fig. 4 (c).

As expected, increasing the flight altitude results in smaller signal powers and therefore in the noisier picture seen in Fig. 10 (e) and (f), but the typical V-shape Doppler chirp which indicates the presence of a target can still clearly be seen in the spectrograms.

Other analysis has shown that, for the conditions used for this experiment, the estimated SNR is approximately 45 dB while the model predicts 47 dB using the effective LPF bandwidth to calculate the noise power.

The two ray path model presented in Section III.B has therefore delivered SNR values which are in good agreement with the measurement results.

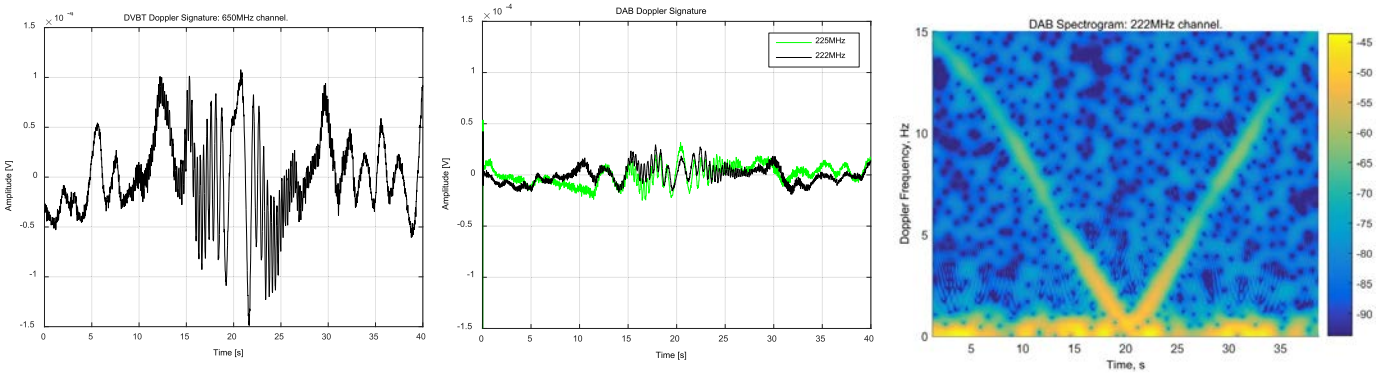

(a) (b) (c)

Figure 9– DVB-T and DAB acquisition of Cessna at 354m above the baseline (D1).

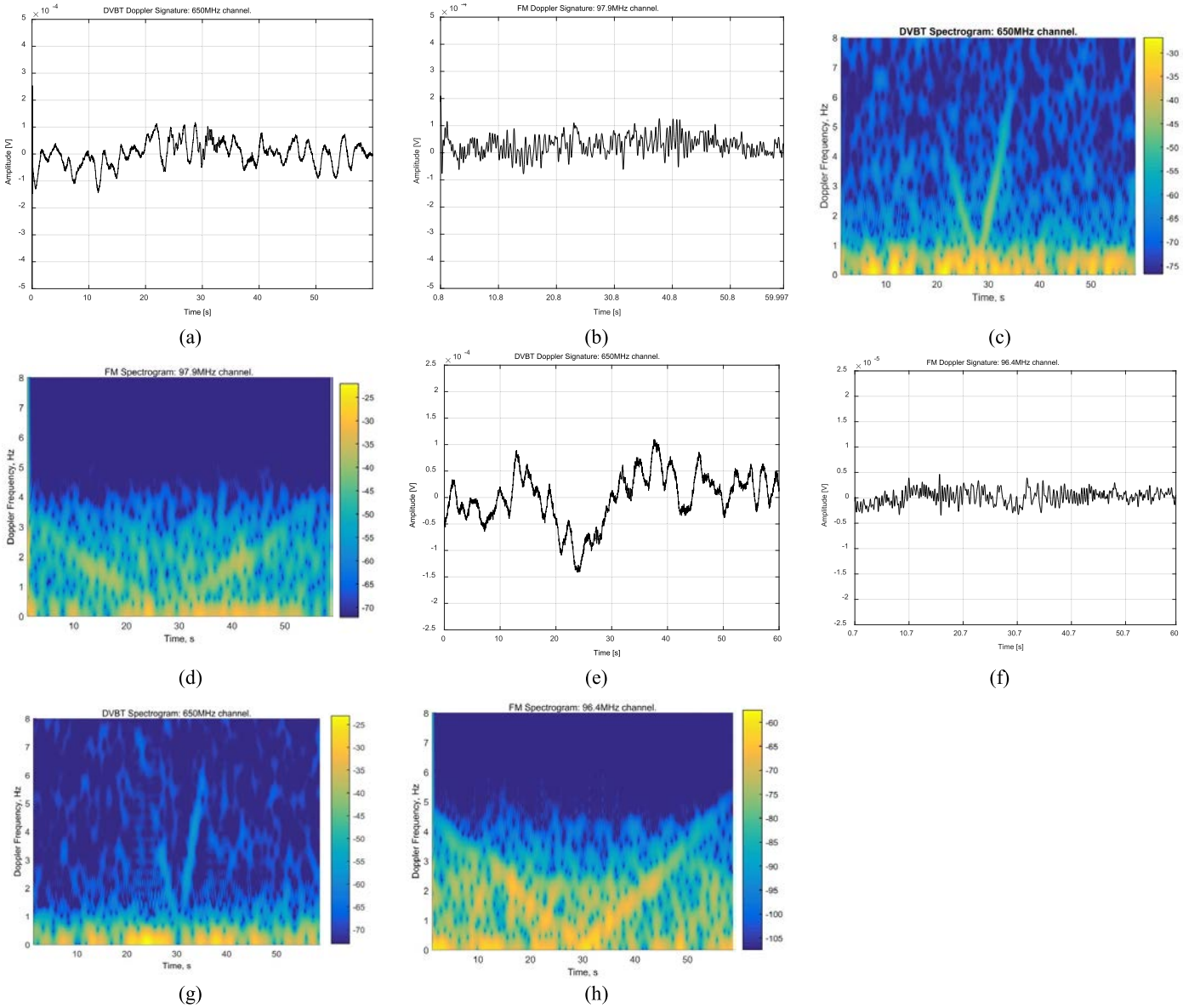

(a) (b) (c)

(d) (e) (f)

(g) (h)

Figure 10 –DVB-T and FM Doppler signatures and spectrograms of Cessna at 659m (a)-(d) and 833m (e)-(h) above the baseline (D2 and D3)

VI. SPEED ESTIMATION

As one of the main drawbacks of FSR is the absence of range resolution, the trajectory parameters of the target cannot be retrieved through the methods used in monostatic and bistatic radar. As discussed above 'SAR like' matched filtering to the possible Doppler trajectories [4] is a quasi-optimal approach which is used to extract these parameters in FSR, where the received target signature is correlated with a bank of waveforms generated for a range of expected values of speed, crossing point and crossing angle.

It was shown in [4] that this procedure is significantly less sensitive to the amplitude of the signature, defined by the FSCS, than it is to the Doppler shifts on the signal. Another way to do this estimation is to use spectrograms directly [28].

Such processing was applied in two cases discussed in the paper: (1) airliner detection by two DVB-T signals presented in Section IV and (2) Cessna detection by DAB and DVB-T as shown in Section V.B. The estimated speeds and those provided by ground truth are given in Table 10 together with the parameters of the signals of opportunity. Very good agreement with ground truth was achieved for both illuminators, for both target types and for both types of ground truth (IFF from Flightradar24 and GPS).

Table 8 – Comparison of speed estimation with sub-optimal processing and ground truth.

DATA	SIGNALS	FREQUENCY MHz	ESTIMATED SPEED km/h	GROUND TRUTH km/h
4	DVB-T	650	248.4	263 by Flightradar 24
	DVB-T	674	216.0	
D2	DAB	222	176.4	167 by GPS
		225	176	
	DVB-T	650	188.1	

VII. CONCLUSIONS AND FUTURE PLANS

In this paper the effectiveness of passive FSR detection has been demonstrated by exploiting broadcast transmitters of opportunity. A simple approach has been proposed to extract the Forward Scatter Doppler signature of target from the signals of terrestrial broadcasting systems, such as DVB-T, DAB and FM. The independence of the FSR signature from the modulation of the transmit signal has been demonstrated both analytically and experimentally. This shows the universality and wide applicability of the FSR approach for target detection in passive coherent location systems.

Experimentation trials have been conducted to study the system performance for a range of different scenarios and airborne targets in multi-frequency/multi-mode setting. The feasibility of a passive FSR for airborne target detection has been demonstrated for the first time using FM, DAB and DVB-T waveforms. It has been shown that simultaneous multi-frequency/multi-band operation increases robustness of detection. While higher frequencies lead to higher accuracy of kinematic parameters estimation, the lower frequency signals define a larger FSR operational region. Moreover, it has been experimentally demonstrated, that the transmitted powers of available Illuminators of Opportunity provide the required sensitivity for detection of airborne targets ranging from an ultralight aircraft to airliners at altitudes up to 1000 m.

In addition, the speed of the detected targets has been estimated using quasi-optimal processing and good correspondence to ground truth data has been demonstrated. This allows the conclusion that P-FSR is a practical solution not only for detection of the target, but also for the estimation of its kinematic parameters. As the next step we plan to investigate the feasibility of extracting kinematic parameters from the spectrograms, which should be more robust to presence of clutter and noise than was the time-domain signature. Furthermore, aircraft target profile reconstruction by its Doppler signature [29] will be investigated.

ACKNOWLEDGEMENTS

This work was supported by UK research council EPSRC within projects EP/L024578/1 and EP/J006610/1.

REFERENCES

[1] M. Cherniakov, "Basic Principles of Forward -Scattering Radars", in *Bistatic Radar: Principles and Practice*, Part III, Wiley, 2007

[2] M. Gashinova, L. Daniel, E. Hoare, V. Sizov, K. Kabakchiev, and M. Cherniakov, "Signal characterisation and processing in the forward scatter mode of bistatic passive coherent location systems", EURASIP Journal on Advances in Signal Processing, vol 2013, no. 1, pp. 1-13, 2013.

[3] M. Cherniakov, "Geometry of Bistatic Radars", in *Bistatic Radar: Principles and Practice,M. Cherniakov*, Part II, Wiley, 2007.

[4] Hu Cheng, V. Sizov, M. Antoniou, M. Gashinova, M. Cherniakov, "Optimal signal processing in ground-based forward scatter micro radars", IEEE Trans. Aerospace Electr. Syst., 2012, vol. 48, (4), pp. 3006–3026.

[5] H. Rohling, '100 years of radar' (Bonn, 2004).

[6] N. Willis, "Forward-Scatter Fences", in *Bistatic Radar*, SciTech Publishing, 2005.

[7] M. Gashinova, L. Daniel, M. Cherniakov, P. Lombardo, D. Pastina, A. De Luca, "Multistatic Forward Scatter Radar for accurate motion parameters estimation of low-observable targets" International Radar Conference 2014, Lille, France, 13-17 October 2014.

[8] D. Pastina, M.Contu, P. Lombardo, M. Gashinova, A. De Luca, L. Daniel, M. Cherniakov "Target motion estimation via multi-node FSR system", (2016) IET Radar, Sonar and Navigation, 10 (1), pp. 3-14.

[9] European Telecommunications Standards Institute, "ETSI EN 300 744, Digital Video Broadcasting (DVB); framing structure, channel coding and modulation for digital terrestrial television," Jan. 2009.

[10] European Telecommunications Standards Institute, “ETSI TS 563, Digital AudioBroadcasting (DAB); Transport of advanced Audio Coding (AAC) audio” Jan. 2009.

[11] S. Haykin, “Frequency Modulation”, in *Communication systems*, Wiley, 2001.

[12] M. Marra, A. De Luca, S. Hristov, L. Daniel, M. Gashinova, M. Cherniakov, “New algorithm for signal detection in passive FSR”, Radar Conference, 27- 30 Oct. 2015, South Africa.

[13] D. E. Hack, L. K. Patton, B. Himed; M. A. Saville, “Detection in Passive MIMO Radar Networks”, IEEE Transaction on Signal Processing, vol. 62, no.11, pp.2999-3012, June 1, 2014.

[14] J. J. Spilker, "Frequency division multiple access and system nonlinearities" in “Digital communication by satellite”, Prentice Hall, 1977.

[15] M. Gashinova, L. Daniel, V. Sizov, E. Hoare, M. Cherniakov, “Phenomenology of Doppler forward scatter radar for surface targets observation”, Radar, Sonar & Navigation, IET, vol.7, (4), pp.422-432, 2013.

[16] N.E.A. Rashid, M. Antoniou, P. Jancovic, V. Sizov, R. Abdullah, M. Cherniakov, “Automatic target classification in a low frequency FSR network”, in Radar Conference, 2008. EuRAD 2008. European, pp.68-71, 30-31 Oct. 2008.

[17] N. Willis, “Doppler resolution”, in *Bistatic Radar* , SciTech Publishing, 2005 .

[18] http://www.CST.com.

[19] V. Sizov, M. Cherniakov, M. Antoniou, “Forward scattering radar power budget analysis for ground targets”, IET Radar Sonar and Navigation, 2007, vol. 1,(6), pp.437-446.

[20] D. W. O’Hagan, H. Kuschel, M. Ummenhofer, J. Heckenbach and J. Schell, 'A Multi-Frequency Hybrid Passive Radar Concept for Medium-Range Air Surveillance' IEEE Aerospace & Electron. Sys. Mag, 2012, vol. 27, (10) pp6-15.

[21] N. Young, R. Hayward and D. Dow 'Multi-Static Primary Surveillance Radar: An Air Navigation Service Provider Perspective,' Proc. Int. Radar Symp. 2015, pp266-71.

[22] https://ukfree.tv/transmitters/tv/Sutton_Coldfield/PGSTART2590/.

[23] National Instruments Corporation 11500 N Mopac Expy, Austin, TX 78759, United States http://www.ni.com/white-paper/52119/en (last access on Nov. 2015).

[24] https://flightradar24.com.

[25] M. Gashinova, V. Sizov; N. A. Zakaria, M. Cherniakov, “Signal detection in multi-frequency Forward Scatter Radar”, inRadar Conference (EuRAD), 2010 European, pp.276-279, Sept. 30 2010-Oct. 1 2010.

[26] M.Gashinova, M. Cherniakov, N.A. Zakaria, V.Sizov, “Empirical Model of Vegetation Clutter in Forward Scatter Radar Micro Sensors”, IEEE Radar Coference 2010, pp.899-904, 10-14May 2010.

[27] http://www.advancednavigation.com.au/product/spatial-dual.

[28] A. De Luca, M. Contu, S.Hiristov, L.Daniel, M.Gashinova, M. Cherniakov, “FSR Velocity Estimation Using Spectrogram”, IRS 2016.

[29] S. Hristov, L. Daniel, E. Hoare, M. Cherniakov, M. Gashinova, “Target Shadow Profile Reconstruction in ground-based forward scatter radar”, in Radar Conference (RadarCon), 2015 IEEE, pp.0846-0851, 10-15 May 2015.